

Propensity Patchwork Kriging for Scalable Inference on Heterogeneous Treatment Effects*

Hajime Ogawa¹ and Shonosuke Sugasawa²

¹Graduate School of Economics, Keio University

²Faculty of Economics, Keio University

Abstract

Gaussian process-based models are attractive for estimating heterogeneous treatment effects (HTE), but their computational cost limits scalability in causal inference settings. In this work, we address this challenge by extending Patchwork Kriging into the causal inference framework. Our proposed method partitions the data according to the estimated propensity score and applies Patchwork Kriging to enforce continuity of HTE estimates across adjacent regions. By imposing continuity constraints only along the propensity score dimension, rather than the full covariate space, the proposed approach substantially reduces computational cost while avoiding discontinuities inherent in simple local approximations. The resulting method can be interpreted as a smoothing extension of stratification and provides an efficient approach to HTE estimation. The proposed method is demonstrated through simulation studies and a real data application.

Key words: Causal inference; Gaussian process; Propensity score; Stratification

*December 30, 2025

1 Introduction

The heterogeneous treatment effect (HTE) is an important concept in causal inference. In many situations such as medicine, marketing and public policy, analysts are interested in knowing the treatment effect at the individual level rather than the entire population or a specific group. Estimating HTE is a challenging problem and several studies have approached this problem using machine learning methods. For example, Louizos et al. (2017) proposed a neural network-based method to adjust for unobserved confounders. In the Bayesian framework, Hahn et al. (2019) proposed Bayesian Causal Forest (BCF), a tree-based model for estimating treatment effects at the individual level. Bayesian methods are advantageous as they allow for the evaluation of uncertainty in HTE estimates. When considering the use of causal inference for individual-level decision-making, the ability to evaluate the uncertainty in HTE estimates is crucial.

In this paper, we focus on methods based on the Gaussian process (GP). GP models are a representative choice for HTE estimation in Bayesian machine learning methods. Alaa and van der Schaar (2017) proposed the *Multi-task Gaussian Process* for factual and counterfactual responses using GP models using a kernel that allows for mutual information sharing. Horii and Chikahara (2023) proposed using GP priors in a *partially linear model* and proved that the posterior of the HTE concentrates around the true one, as the sample size approaches infinity. GP models are highly flexible methods, allowing them to capture nonlinear and complex treatment effects. Furthermore, their smoothness enables the estimation of treatment effects even in situations where the overlap between treatment and control groups is weak (Zhu et al., 2022). A major drawback of Gaussian process (GP) models is their high computational cost. For a sample size n , the computational complexity is generally on the order of $O(n^3)$. Significant research has been dedicated to addressing this issue. One representative approach is the *Sparse Gaussian Process* (Snelson and Ghahramani, 2005), which approximates the covariance matrix using a set of inducing points (pseudo-inputs). Titsias (2009) further advanced this by proposing a

variational inference framework for optimal selection of these inducing points. Another popular category is low-rank approximation. This method approximates the covariance matrix K using a low-rank matrix product QQ^T (Rasmussen and Williams, 2006). Within this approach, the Nyström method (Williams and Seeger, 2000), which uses a subset of data to compute the top eigenvalues for the approximation, is a standard technique. More recently, Datta et al. (2016) proposed the *Nearest Neighbor Gaussian Processes*, which has been extended to various other settings (Finley et al., 2018; Wu et al., 2022).

In this paper, we improve the computational efficiency of GP models for the HTE estimation by introducing *Patchwork Kriging*. The method is based on local approximation, reducing the computational cost by dividing the data into multiple regions. This approach not only reduces computational costs but also allows for region-specific hyperparameter tuning. The main idea of Patchwork Kriging is to obtain a continuous prediction across the boundaries by introducing a latent variable considering the difference between two local models. We propose estimating the propensity score $e(\mathbf{x}) = \mathbb{P}(T = 1|\mathbf{x})$ in advance and using it as the sole partitioning variable in this phase. Our approach extends Patchwork Kriging in that it partitions the data using a one-dimensional variable derived from the features. This idea makes the boundaries between subregions more explicit and helps to address potential imbalances in sample sizes across these regions. Furthermore, our model can be interpreted as a natural extension of stratification in causal inference. In the causal inference framework, stratification methods—which divide the entire dataset into subgroups based on propensity scores and analyze effects within each group—are widely used. This approach has also been extended to the Bayesian framework (McCandless et al., 2009; Orihara and Momozaki, 2024). However, from the perspective of HTE estimation, the results of these methods are discontinuous at the boundary points. Our proposed method mitigates these unnatural discontinuities inherent in conventional methods. A key observation underlying our approach is that, in causal inference, continuity of the heterogeneous treatment effect may not need to be imposed on the entire covariate space. It suffices to ensure smoothness along a one-dimensional balancing

score, such as the propensity score. This allows us to apply Patchwork Kriging in a low-dimensional space, avoiding the geometric and computational challenges of constructing pseudo-observations in high-dimensional input domains. We experimentally demonstrate the efficacy of our proposed method. Simulation studies show that our method is computationally more efficient than standard GP-based baselines and achieves higher accuracy than simple local approximations. Furthermore, in a large-scale real-world application ($N = 7752$), the proposed method reduced the computation time by over three hours compared to the baseline, while effectively mitigating the overfitting typically associated with data partitioning.

The remainder of this paper is organized as follows. In Section 2, we introduce the notation and framework for HTE estimation used in this paper and review the methodology of Patchwork Kriging. Section 3 describes our proposed method, presenting the entire algorithm and the detailed derivation of the target posterior distribution. Section 4 reports the results of simulation studies. We compare the proposed method against a standard GP-based baseline, a simple local approximation of the baseline, and BCF (Hahn et al., 2019), which is a widely used Bayesian machine learning method for HTE estimation. Section 5 presents an empirical application using medical expenditure data to demonstrate the properties of our proposed method. Finally, Section 6 concludes the paper with summary comments.

2 Preliminary

2.1 Notation and framework

This section defines the notation and describes the framework of our model. We consider binary assignment $T \in \{0, 1\}$. The dataset consists of N *i.i.d.* samples $\{\mathbf{x}_n, Y_n, T_n\}_{n=1,\dots,N}$. Let \mathbf{X} be a vector of covariates, and \mathbf{x} be a realization of \mathbf{X} . Our method is based on the *potential outcome framework* (Rubin, 1974). To estimate HTE, we make the following standard assumptions. The first is the *strong ignorability condition*; $\{Y^0, Y^1\} \perp\!\!\!\perp T | \mathbf{X}$.

This assumption is to guarantee independence between potential outcomes and treatment assignment given pre-treatment covariates \mathbf{X} . The second is the *positivity condition*; $0 < \mathbb{P}(T = 1|\mathbf{x}) < 1$. Here, our main interest is estimating HTE on test data.

Our proposed model is a type of *partially linear model* (Engle et al., 1986). The partially linear model is

$$Y = \theta T + f(\mathbf{X}) + \epsilon, \quad \epsilon \sim \mathcal{N}(0, s_\epsilon^{-1})$$

In this model, the baseline of the outcome Y^0 is modeled by a non-linear function $f(\cdot)$ and HTE is represented by a constant parameter θ . In this modeling framework, any suitable type of model could be adapted to $f(\cdot)$. Building on this, Horii and Chikahara (2023) proposed a variant type of the partially linear model

$$Y = \theta(\mathbf{X})T + f(\mathbf{X}) + \epsilon, \quad \epsilon \sim \mathcal{N}(0, s_\epsilon^{-1})$$

In this model, a non-linear function is also adapted to $\theta(\cdot)$, allowing the model to capture complex, individual-level treatment effects. Furthermore, they proposed using zero mean GP prior to both $\theta(\cdot)$ and $f(\cdot)$.

$$\theta(\cdot) \sim \mathcal{GP}(0, C(\cdot, \cdot; \boldsymbol{\omega}_\theta)), \quad f(\cdot) \sim \mathcal{GP}(0, C(\cdot, \cdot; \boldsymbol{\omega}_f))$$

Our proposed model builds upon this formulation. A comparison of experimental results between this baseline model and our proposed model is presented in Section 4.

2.2 Review of Patchwork Kriging

This section reviews *Patchwork Kriging*. First, we consider partitioning the input space of X into K local regions, denoted as $\{\Omega_1, \dots, \Omega_K\}$, with corresponding boundaries $\{\Gamma_{1,2}, \dots, \Gamma_{K,K-1}\}$. Let f_k be the k -th local model which takes an input $x_k \in \Omega_k$. Each local model f_k is assumed to be an mutually independent Gaussian process (GP) with a

zero mean and a covariance function c_k .

The objective of this method is to obtain a continuous prediction across the boundaries. Patchwork Kriging considers the difference between two local models on a shared boundary. Define the latent variable δ as follows;

$$\delta_{k,l}(x) = f_k(x) - f_l(x) \text{ for } x \in \Gamma_{k,l}.$$

To avoid duplication, we assume $k < l$. Note that $\delta_{k,l}$ is the difference between two local models of neighboring regions Ω_k and Ω_l where these areas are in contact $\Gamma_{k,l}$. The key idea of Patchwork Kriging is deriving the posterior predictive distribution by constraining these differences to be zero (i.e., $\delta = 0$). After giving this constraint, initially independent models will be dependent. In practice, since there are infinitely many points on each boundary $\Gamma_{k,l}$, the constraint is enforced on B points randomly sampled from the boundary.

Since our local models are GPs, their difference δ is also a GP. It has a zero mean and a covariance function of $c_k(\cdot, \cdot) + c_l(\cdot, \cdot)$. From the definition of $\delta_{k,l}$, the covariance between $\delta_{k,l}(x_1)$ and $f_j(x_2)$ is given by

$$\begin{aligned} \text{Cov}(\delta_{k,l}(x_1), f_j(x_2)) &= \text{Cov}(f_k(x_1) - f_l(x_1), f_j(x_2)) \\ &= \text{Cov}(f_k(x_1), f_j(x_2)) - \text{Cov}(f_l(x_1), f_j(x_2)) \end{aligned}$$

If $k = j$, $\text{Cov}(f_k(x_1), f_j(x_2)) = c_k(x_1, x_2)$, otherwise take 0. So,

$$\text{Cov}(\delta_{k,l}(x_1), f_j(x_2)) = \begin{cases} c_k(x_1, x_2) & k = j \\ -c_l(x_1, x_2) & l = j \\ 0 & \text{otherwise.} \end{cases} \quad (1)$$

If the local model f_j does not share the boundary $\Gamma_{k,l}$, the covariance takes 0. Similarly,

the covariance between $\delta_{k,l}$ and $\delta_{u,v}$ is

$$\text{Cov}(\delta_{k,l}(x_1), \delta_{u,v}(x_2)) = \begin{cases} c_k(x_1, x_2) & k = u, l \neq v \\ c_l(x_1, x_2) & l = v, k \neq u \\ -c_k(x_1, x_2) & k = v, l \neq u \\ -c_l(x_1, x_2) & l = u, k \neq v \\ c_k(x_1, x_2) + c_l(x_1, x_2) & k = v, l = u \\ 0 & \text{otherwise.} \end{cases} \quad (2)$$

Let x^* be a new input, and we assume $x^* \in \Omega_k$. Additionally, we define δ as the collection of $\delta_{k,l}$. The joint distribution of y , δ and $f_k(x^*)$ is

$$\begin{bmatrix} f_k^* \\ y \\ \delta \end{bmatrix} \sim \mathcal{N} \left(\begin{bmatrix} 0 \\ 0 \\ 0 \end{bmatrix}, \begin{bmatrix} C_{**} & C_{*D} & C_{*\delta} \\ C_{D*} & C_{DD} & C_{D\delta} \\ C_{\delta*} & C_{\delta D} & C_{\delta\delta} \end{bmatrix} \right)$$

Here, we use a local approximation, so C_{DD} is a block diagonal matrix. Also, from (4), $C_{\delta,*}$ is a sparse matrix. For similar reasons, other covariance matrices are sparse matrices too.

Following the standard equations for GP regression, the posterior predictive distribution is Gaussian with the following mean and covariance:

$$\mathbb{E}[f_k^*|y, \delta] = (C_{*D} - C_{*\delta}C_{\delta\delta}^{-1}C_{D\delta}^T)(C_{DD} - C_{D\delta}C_{\delta\delta}^{-1}C_{D\delta}^T)^{-1}y, \quad (3)$$

and

$$\begin{aligned} \text{Cov}(f_k^*|y, \delta) &= C_{**} - C_{*\delta}C_{\delta\delta}^{-1}C_{\delta*}^T \\ &\quad - (C_{*\delta}C_{\delta\delta}^{-1}C_{D\delta}^T)(C_{DD} - C_{D\delta}C_{\delta\delta}^{-1}C_{D\delta}^T)^{-1}(C_{D*} - C_{D\delta}C_{\delta\delta}^{-1}C_{\delta*}^T). \end{aligned} \quad (4)$$

In Patchwork Kriging, the total computational cost is less than standard GP. When calculating (3) or (4), the inversion term $(C_{DD} - C_{D\delta}C_{\delta\delta}^{-1}C_{D\delta}^T)^{-1}$ dominates the overall

computational cost. The total cost is $O(KM^3 + KBM^2 + d_f^3 B^3 K)$, where M is the sample size in each region and d_f is the number of neighboring regions. Typically, $M \simeq N/K$, so computational cost decreases as the number of partitions K increases.

3 Scalable Inference on HTE

A key contribution of our method is an extension of Patchwork Kriging in which continuity constraints are imposed only along the propensity score dimension, rather than over the full covariate space. We refer to this approach as propensity Patchwork Kriging (PPK). We then employ PPK within the partially linear model for HTE estimation. The procedure consists of three main steps. First, we divide the data by propensity score and tune hyperparameters of GP priors in each region. Second, we generate pseudo inputs and constrain their propensity scores to match the boundary values. Finally, we derive posterior predictive distribution by conditioning pseudo observation at the boundaries being equal to zero.

3.1 Dividing data using propensity score

To adapt Patchwork Kriging to our model, we first divide the data. In causal inference, a natural strategy for dividing data is to use propensity score $e(\mathbf{x}) = \mathbb{P}(T = 1|\mathbf{x})$, motivated by propensity score subclassification for causal effect estimation (Rosenbaum and Rubin, 1983). There are two advantages to this method. First, by dividing data using a one-dimensional variable, the boundaries between divided regions become clearer. If we divide data by multiple variables, the connections would be more complex and implementation of Patchwork Kriging would be more difficult as it requires a larger number of pseudo observations under a larger number of boundaries between regions. Pseudo observations act as constraints on the model, thus reducing the number of pseudo observations is preferable. Also, by dividing with multiple variables, a special method is needed to avoid creating regions with small sample size. Park and Apley (2018) used *spatial tree* for each region has the same sample size. However, by dividing with a one-dimensional

variable, such special methods are not needed and we can divide data more easily.

Second, by using propensity score to divide data, our method can be interpreted as a natural extension of stratification methods in causal inference framework. Propensity score is the most popular *balancing score* that constrains $\mathbf{x} \perp\!\!\!\perp T|b(\mathbf{x})$. By combining *strong ignorability*, we can obtain an unbiased estimand of ATE. For this reason, there are many methods that stratify the entire dataset into subgroups and analyze in each group. In HTE estimation, results of these methods are discontinuous at the boundary points. Our proposed method mitigates these unnatural points of conventional method.

3.2 Hyperparameter tuning

In our proposed method, we optimize the hyperparameters of the kernels for $\theta(\cdot)$ and $f(\cdot)$, as well as the noise parameter s_ϵ independently within each local region Ω_k . Specifically, we employ the radial basis function (RBF) kernel for both the treatment effect function $\theta(\cdot)$ and the baseline function $f(\cdot)$, defined as:

$$C(\mathbf{x}, \mathbf{y}) = \exp(-\gamma \|\mathbf{x} - \mathbf{y}\|^2), \quad (5)$$

where $\gamma > 0$ is the parameter that determines the smoothness of the functions. This local optimization allows the model to adapt to region-specific characteristics, such as varying degrees of smoothness (via γ) or noise levels (via s_ϵ).

While various optimization techniques can be employed, we utilize a grid search based on maximum likelihood estimation (MLE). For each local region Ω_k , we maximize the marginal log-likelihood $\mathcal{L}_k(\gamma_\theta, \gamma_f, s_\epsilon)$, defined as

$$\mathcal{L}_k(\gamma_\theta, \gamma_f, s_\epsilon) = \log \mathcal{N}(\mathbf{y}_k | \mathbf{0}, \mathbf{V}_k), \quad \mathbf{V}_k = \text{diag}(\mathbf{t}_k) \mathbf{C}_{\theta,k} \text{diag}(\mathbf{t}_k) + \mathbf{C}_{f,k} + \frac{1}{s_\epsilon} \mathbf{I}_k, \quad (6)$$

where \mathbf{y}_k and \mathbf{t}_k are the vectors of outcomes and treatment assignments for the samples in region Ω_k , respectively. $\mathbf{C}_{\theta,k}$ and $\mathbf{C}_{f,k}$ denote the covariance matrices computed using the RBF kernel (5) within the region.

We choose the set of hyperparameters $(\gamma_\theta, \gamma_f, s_\epsilon)$ from the grid that maximizes (6) for each subregion. It is important to note that this tuning phase is highly computationally efficient, as the optimization for each local region can be executed in parallel. Consequently, the total computational time is significantly lower than that required for a standard global GP model.

3.3 Generation of pseudo data

In this step, we generate pseudo observation at each boundary. The data are already divided into K regions. As we use propensity score as only one-dimensional variable to divide data, the number of boundaries is $K - 1$. We generate B pseudo observations at each boundary, resulting in a total of $B(K - 1)$ additional inputs. The propensity score of each pseudo observation must be constrained to equal the corresponding boundary value. In this work, we use the following procedure.

Here, we describe the generating process for pseudo observations at boundary of the k -th region and $k + 1$ -th region $\mathbf{X}_{b,k,k+1}^{\text{pseudo}}$ for $b \in \{1, \dots, B\}$. We assume \mathbf{X} is a p -dimensional variable. First, we randomly select one dimension to adjust, $p^{\text{adj}} \in \{1, \dots, p\}$. Next, we sample other $p - 1$ dimensions from a normal distribution whose mean and variance parameters are derived from the two neighboring regions.

$$x^j \sim \mathcal{N}(\mu_{k,k+1}^j, (\sigma_{k,k+1}^j)^2), \quad j \in \{1, \dots, p\} \setminus p^{\text{adj}}$$

$$\mu_{k,k+1}^j = \frac{1}{2}\mu_k^j + \frac{1}{2}\mu_{k+1}^j, \quad (\sigma_{k,k+1}^j)^2 = \frac{1}{2}(\sigma_k^j)^2 + \frac{1}{2}(\sigma_{k+1}^j)^2.$$

Finally, we determine the value of the last dimension p^{adj} , such that the propensity score $e(\mathbf{X}_{b,k,k+1}^{\text{pseudo}})$ equals the boundary value. Since we use logistic regression model to estimate propensity score, we can uniquely determine p^{adj} -th variable by using the estimated model parameters.

3.4 Predictive distribution of HTE

In this phase, we construct covariance matrix of prior following the rules of Park and Apley (2018). We consider the partially linear model, $Y = \theta(\mathbf{X})T + f(\mathbf{X}) + \epsilon$. To derive the predictive distribution, we will use following prior.

$$p(\boldsymbol{\Theta}) = p\begin{pmatrix} \boldsymbol{\theta}_n \\ \tilde{\boldsymbol{\theta}}_m \\ \mathbf{f}_n \\ \boldsymbol{\delta} \end{pmatrix} = \mathcal{N}\left(\mathbf{0}, \begin{bmatrix} \Sigma_{\boldsymbol{\theta}_n, \boldsymbol{\theta}_n} & \Sigma_{\boldsymbol{\theta}_n, \tilde{\boldsymbol{\theta}}_m} & \mathbf{0} & \Sigma_{\boldsymbol{\theta}_n, \boldsymbol{\delta}} \\ \Sigma_{\tilde{\boldsymbol{\theta}}_m, \boldsymbol{\theta}_n} & \Sigma_{\tilde{\boldsymbol{\theta}}_m, \tilde{\boldsymbol{\theta}}_m} & \mathbf{0} & \Sigma_{\tilde{\boldsymbol{\theta}}_m, \boldsymbol{\delta}} \\ \mathbf{0} & \mathbf{0} & \Sigma_{\mathbf{f}_n, \mathbf{f}_n} & \mathbf{0} \\ \Sigma_{\boldsymbol{\delta}, \boldsymbol{\theta}_n} & \Sigma_{\boldsymbol{\delta}, \tilde{\boldsymbol{\theta}}_m} & \mathbf{0} & \Sigma_{\boldsymbol{\delta}, \boldsymbol{\delta}} \end{bmatrix}\right). \quad (7)$$

$\boldsymbol{\theta}_n$ and $\tilde{\boldsymbol{\theta}}_m$ are vectors of HTE values evaluated at the training and test input points, respectively. $\boldsymbol{\delta}$ is pseudo observation defined as

$$\boldsymbol{\delta} = \begin{pmatrix} \delta_{1,2} \\ \delta_{2,3} \\ \vdots \\ \delta_{K-1,K} \end{pmatrix} = \begin{pmatrix} \theta^2(\mathbf{X}_{1,1,2}^{\text{pseudo}}) - \theta^1(\mathbf{X}_{1,1,2}^{\text{pseudo}}) \\ \vdots \\ \theta^K(\mathbf{X}_{B,K-1,K}^{\text{pseudo}}) - \theta^{K-1}(\mathbf{X}_{B,K-1,K}^{\text{pseudo}}) \end{pmatrix}$$

$\theta^k(\cdot)$ is HTE function on the k -th region, so $\boldsymbol{\delta}$ is vector of these differences.

Covariance matrices of HTE and nuisance parameter functions $\Sigma_{\boldsymbol{\theta}_n, \boldsymbol{\theta}_n}, \Sigma_{\boldsymbol{\theta}_n, \tilde{\boldsymbol{\theta}}_m}$ and $\Sigma_{\tilde{\boldsymbol{\theta}}_m, \tilde{\boldsymbol{\theta}}_m}$ are block diagonal matrices. For example, if $K = 3$, $\Sigma_{\boldsymbol{\theta}_n, \boldsymbol{\theta}_n}$ is

$$\Sigma_{\boldsymbol{\theta}_n, \boldsymbol{\theta}_n} = \begin{bmatrix} \Sigma_{\boldsymbol{\theta}^1, \boldsymbol{\theta}^1} & \mathbf{0} & \mathbf{0} \\ \mathbf{0} & \Sigma_{\boldsymbol{\theta}^2, \boldsymbol{\theta}^2} & \mathbf{0} \\ \mathbf{0} & \mathbf{0} & \Sigma_{\boldsymbol{\theta}^3, \boldsymbol{\theta}^3} \end{bmatrix}$$

$\Sigma_{\boldsymbol{\theta}^1, \boldsymbol{\theta}^1}$ is kernel matrix for the training data in 1st region. In this work, we set the off-diagonal blocks to 0, making the entire matrix sparse. $\Sigma_{\boldsymbol{\theta}_n, \tilde{\boldsymbol{\theta}}_m}$ and $\Sigma_{\tilde{\boldsymbol{\theta}}_m, \tilde{\boldsymbol{\theta}}_m}$ can be treated similarly.

In the case of $\boldsymbol{\delta}$, unlike the case of the observed data, pseudo-data $\boldsymbol{\delta}_{k,k+1}$ span two

regions, so all the off-diagonal blocks are not imputed with 0. For example, if $K = 4$, it follows from (1) that $\Sigma_{\delta, \theta_n}$ is

$$\Sigma_{\delta, \theta_n} = \begin{bmatrix} \Sigma_{\theta^1, \delta_{1,2}} & \Sigma_{\theta^2, \delta_{1,2}} & \mathbf{0} & \mathbf{0} \\ \mathbf{0} & \Sigma_{\theta^2, \delta_{2,3}} & \Sigma_{\theta^3, \delta_{2,3}} & \mathbf{0} \\ \mathbf{0} & \mathbf{0} & \Sigma_{\theta^3, \delta_{3,4}} & \Sigma_{\theta^4, \delta_{3,4}} \end{bmatrix}.$$

Similarly, covariance matrix $\Sigma_{\delta, \delta}$ is

$$\Sigma_{\delta, \delta} = \begin{bmatrix} \Sigma_{\delta_{1,2}, \delta_{1,2}} & \Sigma_{\delta_{1,2}, \delta_{2,3}} & \mathbf{0} \\ \Sigma_{\delta_{2,3}, \delta_{1,2}} & \Sigma_{\delta_{2,3}, \delta_{2,3}} & \Sigma_{\delta_{2,3}, \delta_{3,4}} \\ \mathbf{0} & \Sigma_{\delta_{3,4}, \delta_{2,3}} & \Sigma_{\delta_{3,4}, \delta_{3,4}} \end{bmatrix}.$$

The computation rule at (2) is a little complicated. However, in this work, we divide the data by a one-dimensional variable, the propensity score, so we use only four cases in (2), diagonal part ($K = v, l = u$), off-diagonal block ($l = u, k \neq v$) or ($k = v, l \neq u$) and 0 part.

Based on the prior construction, we derive the posterior predictive distribution of new input $\tilde{\mathbf{X}}_m$. Our method of derivation is based on Horii and Chikahara (2023). To obtain an analytic formulation of the HTE distribution, we follow three steps. First, we derive joint distribution of outcome of training data \mathbf{y}_n and parameters $\Theta = (\theta_n, \tilde{\theta}_m, f_n, \delta)$. Second, we compute conditional distribution of Θ given \mathbf{y}_n and δ . Finally, we derive the marginal distribution of $\tilde{\theta}_m$.

The joint distribution of \mathbf{y}_n and Θ can be decomposed into the following formulation.

$$p(\mathbf{y}_n, \Theta | \mathbf{x}_n, \tilde{\mathbf{X}}_m) = p(\mathbf{y}_n | \theta_n, \tilde{\theta}_m) p(\Theta | \mathbf{x}_n, \tilde{\mathbf{X}}_m) \quad (8)$$

We have obtained the prior distribution $p(\Theta | \mathbf{x}_n, \tilde{\mathbf{X}}_m)$ in equation (7). The likelihood $p(\mathbf{y}_n | \theta_n, f_n)$ is Gaussian distribution with the mean of $T_n \theta(\mathbf{x}_n) + f(\mathbf{x}_n)$ and the precision of s_ϵ . We assume that hyperparameters of Gaussian process and precision parameter s_ϵ

have already been learned.

To derive the joint distribution, we define $\Sigma_{\Theta, \Theta}$ and $\Delta_{\Theta, \Theta}$ constrain $p(\Theta | \mathbf{x}_n, \tilde{\mathbf{X}}_m) = \mathcal{N}(\mathbf{0}, \Sigma_{\Theta, \Theta})$, $\Delta_{\Theta, \Theta} = \Sigma_{\Theta, \Theta}^{-1}$. $\Sigma_{\Theta, \Theta}$ is covariance matrix define at (7) and $\Delta_{\Theta, \Theta}$ is the precision matrix of $\Sigma_{\Theta, \Theta}$. We can compute $\Delta_{\Theta, \Theta}$ by using the Schur's complement formula.

$$\Delta_{\Theta, \Theta} = \begin{bmatrix} \Delta_{\theta_n, \theta_n} & \Delta_{\theta_n, \tilde{\theta}_m} & \mathbf{0} & \Delta_{\theta_n, \delta} \\ \Delta_{\tilde{\theta}_m, \theta_n} & \Delta_{\tilde{\theta}_m, \tilde{\theta}_m} & \mathbf{0} & \Delta_{\tilde{\theta}_m, \delta} \\ \mathbf{0} & \mathbf{0} & \Delta_{f_n, f_n} & \mathbf{0} \\ \Delta_{\delta, \theta_n} & \Delta_{\delta, \tilde{\theta}_m} & \mathbf{0} & \Delta_{\delta, \delta} \end{bmatrix} \quad (9)$$

By completing the square, we can derive the precision matrix $\hat{\Delta}$ of joint distribution $p(\mathbf{y}_n, \Theta | \mathbf{x}_n, \tilde{\mathbf{X}}_m)$, where the details are provided in the Supplementary Material (Section S1.1). The derivation results are as follows.

$$\begin{aligned} \hat{\Delta} = & \begin{bmatrix} \Delta_{\theta_n, \theta_n} & \mathbf{0} & \mathbf{0} & \mathbf{0} & \mathbf{0} \\ \mathbf{0} & \Delta_{\tilde{\theta}_m, \tilde{\theta}_m} & \mathbf{0} & \mathbf{0} & \mathbf{0} \\ \mathbf{0} & \mathbf{0} & \Delta_{f_n, f_n} & \mathbf{0} & \mathbf{0} \\ \mathbf{0} & \mathbf{0} & \mathbf{0} & \Delta_{\delta, \delta} & \mathbf{0} \\ \mathbf{0} & \mathbf{0} & \mathbf{0} & \mathbf{0} & s_\epsilon \mathbf{I}_n \end{bmatrix} \\ & + \begin{bmatrix} s_\epsilon \mathbf{T}_n^2 & \Delta_{\theta_n, \tilde{\theta}_m} & \mathbf{T}_n^T s_\epsilon & \Delta_{\theta_n, \delta} & -s_\epsilon \mathbf{T}_n \\ \Delta_{\tilde{\theta}_m, \theta_n} & \mathbf{0} & \mathbf{0} & \Delta_{\tilde{\theta}_m, \delta} & \mathbf{0} \\ \mathbf{T}_n^T s_\epsilon & \mathbf{0} & s_\epsilon \mathbf{I}_n & \mathbf{0} & -s_\epsilon \mathbf{I}_n \\ \Delta_{\delta, \theta_n} & \Delta_{\delta, \tilde{\theta}_m} & \mathbf{0} & \mathbf{0} & \mathbf{0} \\ -s_\epsilon \mathbf{I}_n \mathbf{T}_n & \mathbf{0} & -s_\epsilon \mathbf{I}_n & \mathbf{0} & \mathbf{0} \end{bmatrix} \end{aligned} \quad (10)$$

We define the inverse matrix of this distribution as $\hat{\Sigma} = \hat{\Delta}^{-1}$. $\hat{\Sigma}$ is covariance matrix of (8). This procedure is computationally expensive, so we compute the inverse matrix by block decomposition method, where the details are provided in the Supplementary Material (Section S1.2).

Next, we derive the conditional distribution $p(\hat{\Theta} | \mathbf{y}_n, \delta, \mathbf{X}_n, \tilde{\mathbf{X}}_m)$. To do so, let $\hat{\Sigma}$ be

a covariance matrix of $p(\Theta, \mathbf{y}_n, \delta | \mathbf{X}_n, \tilde{\mathbf{X}}_m)$.

$$\hat{\Sigma} = \begin{bmatrix} \hat{\Sigma}_{\Theta, \Theta} & \hat{\Sigma}_{\Theta, D} \\ \hat{\Sigma}_{D, \Theta} & \hat{\Sigma}_{D, D} \end{bmatrix}$$

where $\hat{\Sigma}_{\Theta, \Theta}$, $\hat{\Sigma}_{D, D}$ and $\hat{\Sigma}_{\Theta, D}$ are the covariance matrices corresponding to the variance of $\hat{\Theta} = (\theta_n, \tilde{\theta}_m, \mathbf{f}_n)^T$, the variance of $D = (\delta, \mathbf{y}_n)^T$ and covariance between $\hat{\Theta}$ and D respectively. Using the standard formulas for conditional Gaussian distributions, the distribution of $\hat{\Theta}$ conditioned on D is derived as follows.

$$p(\hat{\Theta} | \mathbf{y}_n, \delta = 0, \mathbf{x}_n, \tilde{\mathbf{X}}_m) = \mathcal{N}(\boldsymbol{\mu}_{\Theta|D}, \Sigma_{\Theta|D}) \quad (11)$$

with $\boldsymbol{\mu}_{\Theta|D} = MD$ and $\Sigma_{\Theta|D} = \hat{\Sigma}_{\Theta, \Theta} - M\hat{\Sigma}_{D, \Theta}$, where

$$M = \hat{\Sigma}_{\Theta, D} \hat{\Sigma}_{D, D}^{-1} = \begin{pmatrix} M_{\theta_n} \\ M_{\tilde{\theta}_m} \\ M_{\mathbf{f}_n} \end{pmatrix}, \quad D = \begin{pmatrix} \delta \\ \mathbf{y}_n \end{pmatrix} = \begin{pmatrix} \mathbf{0} \\ \mathbf{y}_n \end{pmatrix}$$

This distribution is joint posterior given data \mathbf{y}_n and constraint $\delta = 0$. Note that the posterior mean $\boldsymbol{\mu}_{\Theta|D}$ is a vector partitioned into three blocks, and the posterior covariance $\Sigma_{\Theta|D}$ is 3×3 block matrix.

Finally, our main target predictive distribution of HTE on the test data $\tilde{\theta}_m$ is obtained by marginalizing the joint posterior distribution (11) except for $\tilde{\theta}_m$. The resulting distribution is

$$p(\tilde{\theta}_m) = \mathcal{N}(M_{\tilde{\theta}_m} D, \Sigma_{\tilde{\theta}_m, \tilde{\theta}_m|D})$$

where $\Sigma_{\tilde{\theta}_m, \tilde{\theta}_m|D}$ is $(2, 2)$ -block of the $\Sigma_{\Theta|D}$ at (11). If we are concerned with the distribution of $\tilde{\theta}_m$ only, we calculate only the blocks that are needed in M , $\boldsymbol{\mu}_{\Theta|D}$, and $\Sigma_{\Theta|D}$.

4 Experiments

In this section, we conduct simulation studies to evaluate the performance of our proposed model. The objective of the experiments is to estimate the HTE on synthetic data. The data generation process of experiments is adapted from Nie and Wager (2020). We conducted simulation studies on four scenarios. In all settings, the covariates are set as $x \in \mathcal{R}^6$ and data-generating processes are complicated. We set sample size of training data to $N = \{200, 500, 1000\}$ and in any case, we set test data at $M = 500$. The entire process, from data generation to inference, was repeated 100 times in each scenario. Further details are provided in the Supplementary Material (Section S2). We here show two scenarios, Setup A and Setup C. In Setup A, the true HTE function and the true propensity score both depend on X_1 and X_2 , whereby data dividing using estimated propensity score is expected to be effective. In Setup C, the true HTE function is constant at 1, so the dividing method itself is not considered to be effective.

In this study, we use the partially linear model with GP as the baseline method. Furthermore, we compare simple local approximation of the baseline model. Here, data dividing method and tuning of hyperparameter of local approximation are identical to those of our proposed model. When the data are divided to K regions, we use common estimated propensity scores in the local approximation. We set the number of regions to $K = \{2, 5, 10\}$. When we tune the hyperparameters of each local model, this step was carried out by using a parallel computer with 10 threads. We performed a grid search in the range $(0.1, 5.0)$ with a step size of 0.2 as the GP's hyperparameter. In addition, we compare *Bayesian Causal Forest* (BCF) (Hahn et al., 2019) as a Bayesian machine learning method other than GP. All computations were carried out on a workstation with 12th Gen Intel Core i7-12650H processor (16 logical cores) and 32.0 GB of RAM.

In Figure 1, we show comparison of MSE. Note that in almost all cases, PPK outperforms simple local approximation for the same sample size and number of regions. The only cases where PPK is not explicitly better than local approximation in Setup C with

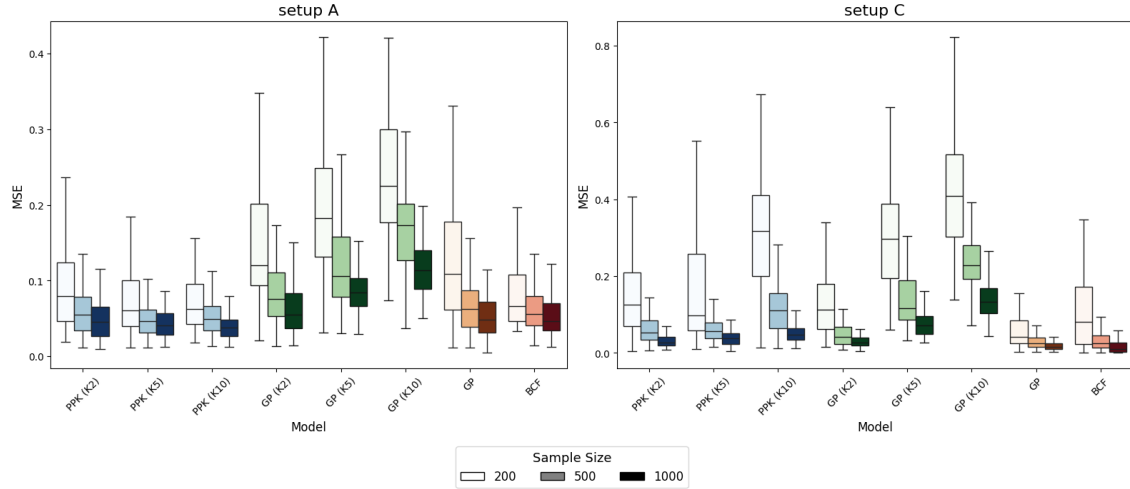


Figure 1: MSEs on settings A and C

$K = 2$. In $K = 2$ case, the number of boundaries between regions is only one, so effect of the *patchwork* scheme is expected to be weaker than in the $K = 5$ or 10 cases. In divided region, local model can only use smaller sample than baseline model, but the negative effect appears to be relatively small. Our proposed model and local approximation can use hyperparameters different for each region. A key advantage of this approach is that, unlike the baseline global GP, it allows for region-specific hyperparameters. This flexibility enables the model to capture locally varying patterns and smoothness. Consequently, the negative effect of smaller local sample sizes is mitigated by this adaptability.

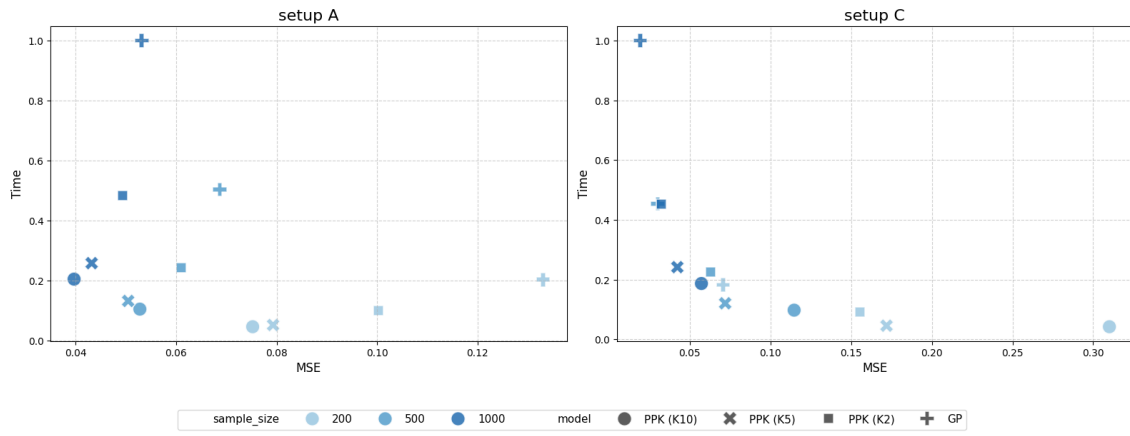


Figure 2: Computation time and MSEs on settings A and C

As shown in Figure 2, the computation times do not differ significantly between Setup A and C. The parallelized hyperparameter tuning contributes the most to the reduction

in computation time. For smaller sample sizes, the benefit of increasing the number of partitions is less pronounced due to the overhead associated with parallelization. No model achieves the nominal coverage probability across all scenarios. The interval length primarily depends on the sample size of each region; thus, local models in regions with fewer samples produce wider intervals.

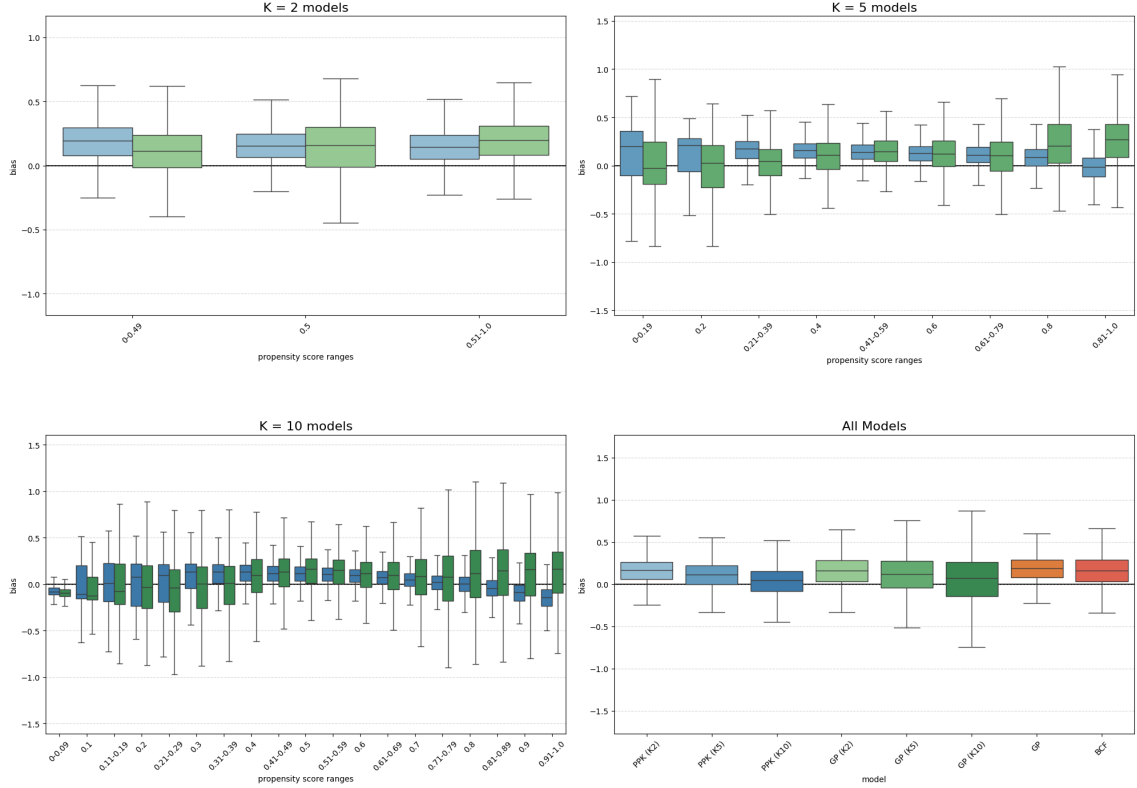


Figure 3: Comparison of HTE estimation bias near partition boundaries on Setup A. The plots show the average bias for data points within a ± 0.01 margin of the specified split points. The panels represent $K = 2$ (top-left), $K = 5$ (top-right), and $K = 10$ (bottom-left), with the bottom-right panel summarizing the bias across all K settings and other methods.

Furthermore, we conducted an additional simulation study to specifically evaluate the bias of the HTE estimates at the subregion boundaries. In the previous experiments, data partitioning was determined by the quantiles of the estimated propensity score. In this setting, however, we partitioned the data at fixed, predetermined values to explicitly examine behavior around the boundaries. Specifically, we set the cutoff values at $\{0.5\}$ for $K = 2$, $\{0.2, 0.4, 0.6, 0.8\}$ for $K = 5$, and $\{0.1, 0.2, \dots, 0.9\}$ for $K = 10$. To assess the

local performance near these boundaries, we calculated the bias for data points located within a margin of ± 0.01 of each boundary and each local region. Figure 3 shows that PPK is less prone to significant bias at each local region and the boundaries compared to the simple local approximation. In the latter approach, each local model is fitted independently within its local regions and are likely to result in overfitting. Also, because local approximation methods join the overfitting local models without consideration of discontinuities, they are prone to significant bias at the boundaries.

5 Application: The Effect of Smoking on Medical Expenditures

5.1 Data

Here, we consider a real world analysis that infers the effect of smoking on medical expenditures as an application. This problem has been analyzed in several papers. We use the data from the 1987 National Medical Expenditures Survey (NMES) by Johnson et al. (2003). The dataset was constructed following the procedure in Imai and van Dyk (2004), resulting in a sample size of $N = 7752$. The dataset includes the following 10 covariates:

- **age:** age in years at the time of the survey
- **smoke age:** age in years when the individual started smoking
- **gender:** male or female
- **race:** other, black or white
- **marriage status:** married, widowed, divorced, separated, never married
- **education level:** college graduate, some college, high school graduate, other
- **census region:** geographic location, Northeast, Midwest, South, West
- **poverty status:** poor, near poor, low income, middle income, high income
- **seat belt:** does patient regularly use a seat belt when in a car
- **years quit:** how many years since the individual quit smoking.

The outcome is the logarithm of annual medical expenditures. To treat the intervention as binary, following Hahn et al. (2019), we assign $T_i = 1$ to unit i if their *pack-years* exceed 17, and $T_i = 0$ otherwise. This variable is interpreted as the cumulative amount of smoking; See Imai and van Dyk (2004) for further details.

In this application, as in the simulation study, we use PPK, the baseline GP model, a simple local approximation of the baseline and BCF. Due to the larger sample size, we increase the number of regions K to $\{10, 30, 45\}$ and set the number of pseudo observations at each boundary B to 20. We performed a grid search in the range $(0.1, 10.0)$ with a step size of 0.2 as the GP's hyperparameter.

5.2 Results

First, we examine the relationship between the estimated HTE and the propensity scores. Figure 4 displays the spline-smoothed trends for each method, overlaid with the scatter plot of the estimated results of the HTE from PPK ($K = 30$). We confirm that the trend of PPK closely matches that of the simple local approximation with the same number of regions. In contrast, the estimated HTE for the baseline GP model and BCF show constant behavior with respect to the propensity scores, because they are not divided by the propensity scores.

Second, although the overall spline trends match between PPK and local approximation, there are significant differences at the individual level. Figure 5 shows the scatter plots of the estimates from our proposed method ($K = 30$) and the local approximation ($K = 30$). While the latter plot exhibits distinct discontinuities between divided regions like blocks, the former shows these blocks connected more smoothly across boundaries. Furthermore, Figure 6 shows the overlap of these estimates. The simple local approximation fits the model using only the limited number of samples within each divided region, making it prone to overfitting. As seen in Figure 6, the "red blocks" (local approximation) exhibit high variance, deviating significantly above and below the "blue blocks" (PPK).

Finally, we compare the computation times. Due to the data partitioning strategy, all

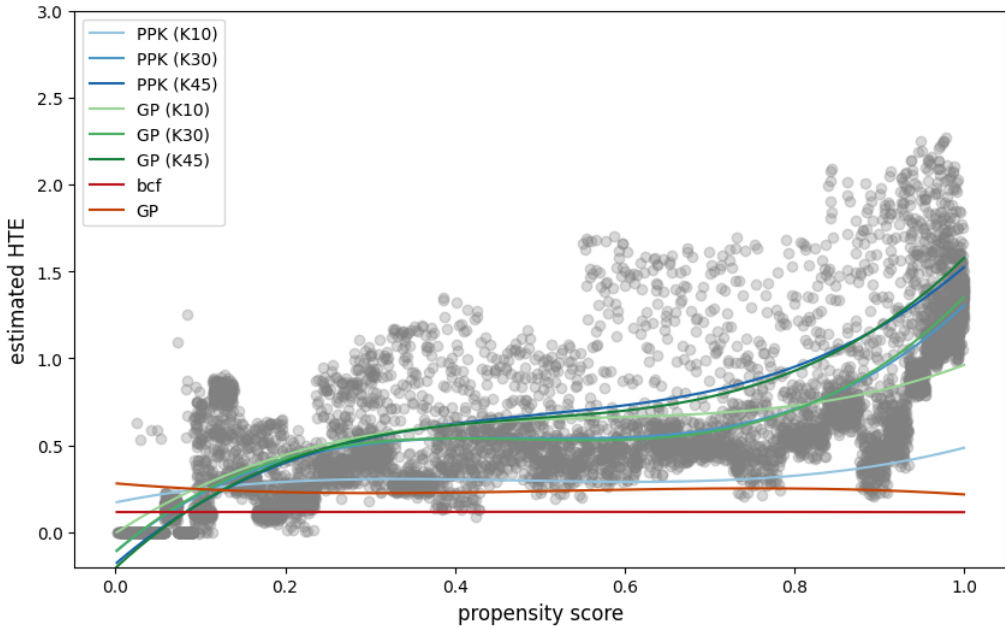


Figure 4: Spline-smoothed trends of estimated HTE versus propensity scores. Gray dots indicate the estimates from the proposed method ($K = 30$).

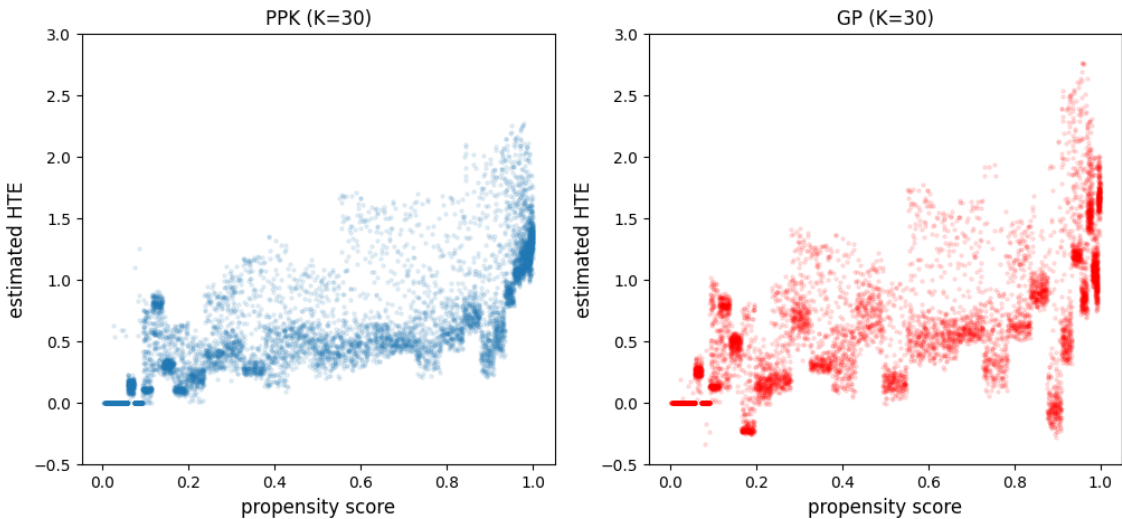


Figure 5: Scatter plots of estimated HTE versus propensity scores: (Left) Proposed method (PPK) and (Right) the simple local approximation (GP).

proposed methods achieve a reduction in computation time compared to the baseline GP model. Note that the experiments were conducted on a CPU with 16 threads, with the maximum number of parallel processes set to 15 for hyperparameter tuning. In the case of $K = 10$, all regions can be tuned simultaneously. However, for $K = 45$, the tuning process requires at least three sequential batches (since $45/15 = 3$). Although increasing

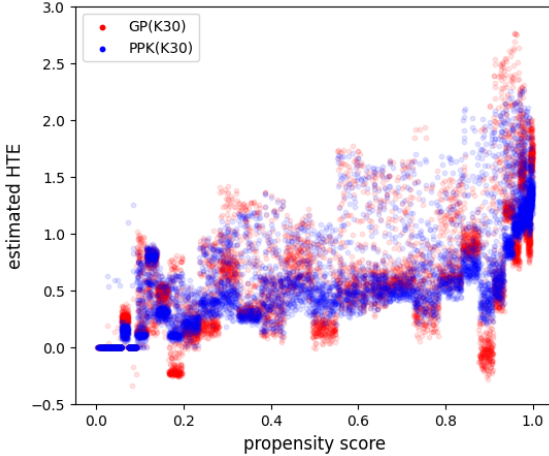


Figure 6: Overlapped scatter plot of the estimates shown in Figure 5.

the number of regions reduces the computation time for each individual region, the limited number of cores prevents us from fully benefiting from parallelization in the $K = 45$ case.

Table 1: Computation time (sec) for each method

	PPK (K10)	PPK (K30)	PPK (K45)	GP
Time (sec)	2912	2473	2496	14534

6 Concluding Remarks

In this paper, we proposed propensity Patchwork Kriging, an efficient HTE estimation method using Gaussian Processes (GP) combined with the Patchwork Kriging technique. Our experiments demonstrated that PPK is computationally more efficient than standard GP approaches, and more accurate than simple local approximation methods. Depending on the DGP, partitioning the data proved effective because it allows for hyperparameter tuning specific to each local region. A key feature of our approach is the use of estimated propensity scores for data partitioning. By utilizing this one-dimensional variable, the boundaries between regions become clearer, simplifying the subsequent implementation. Furthermore, PPK can be interpreted as a natural extension of stratification methods within the causal inference framework.

Acknowledgement

This work is partially supported by JSPS KAKENHI Grant Numbers 24K21420 and 25H00546.

References

- Alaa, A. M. and M. van der Schaar (2017). Bayesian inference of individualized treatment effects using multi-task gaussian processes. In I. Guyon, U. V. Luxburg, S. Bengio, H. Wallach, R. Fergus, S. Vishwanathan, and R. Garnett (Eds.), *Advances in Neural Information Processing Systems*, Volume 30. Curran Associates, Inc.
- Datta, A., S. Banerjee, A. O. Finley, and A. E. Gelfand (2016). Hierarchical nearest-neighbor gaussian process models for large geostatistical datasets. *Journal of the American Statistical Association* 111(514), 800–812. PMID: 29720777.
- Engle, R. F., C. W. J. Granger, J. Rice, and A. Weiss (1986). Semiparametric estimates of the relation between weather and electricity sales. *Journal of the American Statistical Association* 81(394), 310–320.
- Finley, A. O., A. Datta, B. C. Cook, D. C. Morton, H. E. Andersen, and S. Banerjee (2018). Efficient algorithms for bayesian nearest neighbor gaussian processes.
- Hahn, P. R., J. S. Murray, and C. Carvalho (2019). Bayesian regression tree models for causal inference: regularization, confounding, and heterogeneous effects.
- Horii, S. and Y. Chikahara (2023). Uncertainty quantification in heterogeneous treatment effect estimation with gaussian-process-based partially linear model.
- Imai, K. and D. A. van Dyk (2004). Causal inference with general treatment regimes. *Journal of the American Statistical Association* 99(467), 854–866.

- Johnson, E., F. Dominici, M. Griswold, and S. L. Zeger (2003). Disease cases and their medical costs attributable to smoking: an analysis of the national medical expenditure survey. *Journal of Econometrics* 112(1), 135–151. Analysis of data on health: 2.
- Louizos, C., U. Shalit, J. Mooij, D. Sontag, R. Zemel, and M. Welling (2017). Causal effect inference with deep latent-variable models.
- McCandless, L. C., P. Gustafson, and P. C. Austin (2009). Bayesian propensity score analysis for observational data. *Statistics in Medicine* 28(1), 94–112.
- Nie, X. and S. Wager (2020). Quasi-oracle estimation of heterogeneous treatment effects.
- Orihara, S. and T. Momozaki (2024). Bayesian-based propensity score subclassification estimator.
- Park, C. and D. Apley (2018). Patchwork kriging for large-scale gaussian process regression.
- Rasmussen, C. E. and C. K. I. Williams (2006). *Gaussian Processes for Machine Learning*. The MIT Press.
- Rosenbaum, P. R. and D. B. Rubin (1983). The central role of the propensity score in observational studies for causal effects. *Biometrika* 70(1), 41–55.
- Rubin, D. (1974). Estimating causal effects of treatments in randomized and nonrandomized studies. *Journal of Educational Psychology* 66, 688–701.
- Snelson, E. and Z. Ghahramani (2005). Sparse gaussian processes using pseudo-inputs. In Y. Weiss, B. Schölkopf, and J. Platt (Eds.), *Advances in Neural Information Processing Systems*, Volume 18. MIT Press.
- Titsias, M. (2009, 16–18 Apr). Variational learning of inducing variables in sparse gaussian processes. In D. van Dyk and M. Welling (Eds.), *Proceedings of the Twelfth International Conference on Artificial Intelligence and Statistics*, Volume 5 of *Proceedings*

of Machine Learning Research, Hilton Clearwater Beach Resort, Clearwater Beach, Florida USA, pp. 567–574. PMLR.

Williams, C. and M. Seeger (2000). Using the nyström method to speed up kernel machines. In T. Leen, T. Dietterich, and V. Tresp (Eds.), *Advances in Neural Information Processing Systems*, Volume 13. MIT Press.

Wu, L., G. Pleiss, and J. P. Cunningham (2022). Variational nearest neighbor gaussian processes. *CoRR abs/2202.01694*.

Zhu, Y., N. Mitra, and J. Roy (2022). Addressing positivity violations in causal effect estimation using gaussian process priors.

Supplementary Material for ‘‘Propensity Patchwork Kriging for Scalable Inference on Heterogeneous Treatment Effects’’

This Supplementary Material provides details about derivation of proposed method, data generation process of simulation study, and additional simulation results.

S1 Details of Derivation

S1.1 Prior precision matrix

In section 2.3.3, we provide a detailed derivation of prior precision matrix of Θ in (9). We defined the precision matrix as the inverse of covariance matrix, $\Delta_{\Theta,\Theta} = \Sigma_{\Theta,\Theta}^{-1}$, where $\Sigma_{\Theta,\Theta}$ is covariance matrix from (7). To compute the inverse of this block matrix, we use the Schur’s complement as follows;

$$\begin{bmatrix} A & B \\ C & D \end{bmatrix}^{-1} = \begin{bmatrix} M^{-1} & -M^{-1}BD^{-1} \\ -D^{-1}CM^{-1} & D^{-1} + D^{-1}CM^{-1}BD^{-1} \end{bmatrix} \quad (\text{S1})$$

$$M = A - BD^{-1}C$$

The precision matrix is inverse of 4×4 block matrix.

$$\Delta_{\Theta,\Theta} = \Sigma_{\Theta,\Theta}^{-1} = \begin{bmatrix} \Sigma_{\theta_n,\theta_n} & \Sigma_{\theta_n,\tilde{\theta}_m} & \mathbf{0} & \Sigma_{\theta_n,\delta} \\ \Sigma_{\tilde{\theta}_m,\theta_n} & \Sigma_{\tilde{\theta}_m,\tilde{\theta}_m} & \mathbf{0} & \Sigma_{\tilde{\theta}_m,\delta} \\ \mathbf{0} & \mathbf{0} & \Sigma_{f_n,f_n} & \mathbf{0} \\ \Sigma_{\delta,\theta_n} & \Sigma_{\delta,\tilde{\theta}_m} & \mathbf{0} & \Sigma_{\delta,\delta} \end{bmatrix}^{-1}$$

To apply the formula (S1), we partition $\Sigma_{\Theta,\Theta}$ by defining A as the upper-left 3×3 block, B as the upper-right 3×1 block, C as the lower-left 1×3 block, and D as the scalar block $\Sigma_{\delta,\delta}$.

First, we compute the term $BD^{-1}C$:

$$\begin{aligned}
BD^{-1}C &= \begin{bmatrix} \Sigma_{\theta_n, \delta} \\ \Sigma_{\tilde{\theta}_m, \delta} \\ \mathbf{0} \end{bmatrix} \Sigma_{\delta, \delta}^{-1} \begin{bmatrix} \Sigma_{\delta, \theta_n} & \Sigma_{\delta, \tilde{\theta}_m} & \mathbf{0} \end{bmatrix} \\
&= \begin{bmatrix} \Sigma_{\theta_n, \delta} \Sigma_{\delta, \delta}^{-1} \Sigma_{\delta, \theta_n} & \Sigma_{\theta_n, \delta} \Sigma_{\delta, \delta}^{-1} \Sigma_{\delta, \tilde{\theta}_m} & \mathbf{0} \\ \Sigma_{\tilde{\theta}_m, \delta} \Sigma_{\delta, \delta}^{-1} \Sigma_{\delta, \theta_n} & \Sigma_{\tilde{\theta}_m, \delta} \Sigma_{\delta, \delta}^{-1} \Sigma_{\delta, \tilde{\theta}_m} & \mathbf{0} \\ \mathbf{0} & \mathbf{0} & \mathbf{0} \end{bmatrix}
\end{aligned}$$

Next, we compute M in (S1):

$$\begin{aligned}
M &= A - BD^{-1}C \\
&= \begin{bmatrix} \Sigma_{\theta_n, \theta_n} - \Sigma_{\theta_n, \delta} \Sigma_{\delta, \delta}^{-1} \Sigma_{\delta, \theta_n} & \Sigma_{\theta_n, \tilde{\theta}_m} - \Sigma_{\theta_n, \delta} \Sigma_{\delta, \delta}^{-1} \Sigma_{\delta, \tilde{\theta}_m} & \mathbf{0} \\ \Sigma_{\tilde{\theta}_m, \theta_n} - \Sigma_{\tilde{\theta}_m, \delta} \Sigma_{\delta, \delta}^{-1} \Sigma_{\delta, \theta_n} & \Sigma_{\tilde{\theta}_m, \tilde{\theta}_m} - \Sigma_{\tilde{\theta}_m, \delta} \Sigma_{\delta, \delta}^{-1} \Sigma_{\delta, \tilde{\theta}_m} & \mathbf{0} \\ \mathbf{0} & \mathbf{0} & \Sigma_{f_n, f_n} \end{bmatrix}.
\end{aligned}$$

To compute the inverse of M , we use (S1) repeatedly. Let A' be the upper-left 2×2 block, B' as 2×1 , C' as lower-right 1×2 block and D' as Σ_{f_n, f_n} . Notice that off-diagonal matrices B' and C' are zero-matrix. Also, let A'' through D'' denote the blocks of A'

Because B' and C' are zero-matrices, applying (S1) to M , M^{-1} is a block diagonal matrix as follows:

$$\begin{aligned}
M^{-1} &= \begin{bmatrix} A'^{-1} & \mathbf{0} \\ \mathbf{0} & D'^{-1} \end{bmatrix} = \begin{bmatrix} M'' & -M''^{-1} B'' C'' & \mathbf{0} \\ -D^{-1} C'' M''^{-1} & D''^{-1} - D^{-1} C'' M''^{-1} B D^{-1} & \mathbf{0} \\ \mathbf{0} & \mathbf{0} & \Sigma_{f_n, f_n}^{-1} \end{bmatrix} \\
&\equiv \begin{bmatrix} \Delta_{\theta_n, \theta_n} & \Delta_{\theta_n, \tilde{\theta}_m} & \mathbf{0} \\ \Delta_{\tilde{\theta}_m, \theta_n} & \Delta_{\tilde{\theta}_m, \tilde{\theta}_m} & \mathbf{0} \\ \mathbf{0} & \mathbf{0} & \Delta_{f_n, f_n} \end{bmatrix},
\end{aligned}$$

where $M'' = A'' - B''D''^{-1}C''$.

Now we compute the upper-right blocks in the (S1) to obtain

$$-M^{-1}BD^{-1} = \begin{bmatrix} -(\Delta_{\theta_n, \theta_n} \Sigma_{\theta_n, \delta} + \Delta_{\theta_n, \tilde{\theta}_m} \Sigma_{\tilde{\theta}_m, \delta}) \Sigma_{\delta, \delta}^{-1} \\ -(\Delta_{\tilde{\theta}_m, \theta_n} \Sigma_{\theta_n, \delta} + \Delta_{\tilde{\theta}_m, \tilde{\theta}_m} \Sigma_{\tilde{\theta}_m, \delta}) \Sigma_{\delta, \delta}^{-1} \\ \mathbf{0} \end{bmatrix} \equiv \begin{bmatrix} \Delta_{\theta_n, \delta} \\ \Delta_{\tilde{\theta}_m, \delta} \\ \mathbf{0} \end{bmatrix} \quad (\text{S2})$$

The lower-left block in (S1) is the transpose of (S2), obtained as

$$\begin{aligned} & -D^{-1}CM^{-1} \\ &= \begin{bmatrix} -\Sigma_{\delta, \delta}^{-1}(\Sigma_{\delta, \theta_n} \Delta_{\theta_n, \theta_n} + \Sigma_{\delta, \tilde{\theta}_m} \Delta_{\tilde{\theta}_m, \theta_n}) & -\Sigma_{\delta, \delta}^{-1}(\Sigma_{\delta, \theta_n} \Delta_{\theta_n, \tilde{\theta}_m} + \Sigma_{\delta, \tilde{\theta}_m} \Delta_{\tilde{\theta}_m, \tilde{\theta}_m}) & \mathbf{0} \\ \Delta_{\delta, \theta_n} & \Delta_{\delta, \tilde{\theta}_m} & \mathbf{0} \end{bmatrix} \\ & \equiv \begin{bmatrix} \Delta_{\delta, \theta_n} & \Delta_{\delta, \tilde{\theta}_m} & \mathbf{0} \end{bmatrix} \end{aligned}$$

The lower-right block is scalar block as follows:

$$\begin{aligned} D^{-1} + D^{-1}CM^{-1}BD^{-1} &= \Sigma_{\delta, \delta} - (\Delta_{\delta, \theta_n} \Sigma_{\theta_n, \delta} + \Delta_{\delta, \tilde{\theta}_m} \Sigma_{\tilde{\theta}_m, \delta}) \Sigma_{\delta, \delta}^{-1} \\ & \equiv \Delta_{\delta, \delta} \end{aligned}$$

S1.2 Joint covariance matrix

This section details the derivation of $\hat{\Sigma} = \hat{\Delta}^{-1}$, which is the covariance matrix of the joint distribution $p(\Theta, \mathbf{y}_n, \delta | \mathbf{X}_n, \tilde{\mathbf{X}}_m)$. We have defined $\hat{\Delta}$ as (10). To compute the inverse matrix, we use Schur's complement (S1) repeatedly, as in Section A.1.

From the definition, the precision matrix $\hat{\Delta}$ is a 5×5 block matrix.

$$\hat{\Delta} = \begin{bmatrix} \Delta_{\theta_n, \theta_n} + s_\epsilon \mathbf{T}_n^2 & \Delta_{\theta_n, \tilde{\theta}_m} & \mathbf{T}_n^T s_\epsilon & \Delta_{\theta_n, \delta} & -s_\epsilon \mathbf{T}_n \\ \Delta_{\tilde{\theta}_m, \theta_n} & \Delta_{\tilde{\theta}_m, \tilde{\theta}_m} & \mathbf{0} & \Delta_{\tilde{\theta}_m, \delta} & \mathbf{0} \\ \mathbf{T}_n^T s_\epsilon & \mathbf{0} & \Delta_{\mathbf{f}_n, \mathbf{f}_n} + s_\epsilon \mathbf{I}_n & \mathbf{0} & -s_\epsilon \mathbf{I}_n \\ \Delta_{\delta, \theta_n} & \Delta_{\delta, \tilde{\theta}_m} & \mathbf{0} & \Delta_{\delta, \delta} & \mathbf{0} \\ -s_\epsilon \mathbf{I}_n \mathbf{T}_n & \mathbf{0} & -s_\epsilon \mathbf{I}_n & \mathbf{0} & s_\epsilon \mathbf{I}_n \end{bmatrix}$$

To apply the formula (S1), we partition the matrix by defining A as the upper-left 4×4 block, B as the upper-right 4×1 block, C as the lower-left 1×4 block, and D as the scalar block $s_\epsilon \mathbf{I}_n$. Next, we compute M in (S1).

$$M = A - BD^{-1}C$$

$$= \begin{bmatrix} \Delta_{\theta_n, \theta_n} & \Delta_{\theta_n, \tilde{\theta}_m} & \mathbf{0} & \Delta_{\theta_n, \delta} \\ \Delta_{\tilde{\theta}_m, \theta_n} & \Delta_{\tilde{\theta}_m, \tilde{\theta}_m} & \mathbf{0} & \Delta_{\tilde{\theta}_m, \delta} \\ \mathbf{0} & \mathbf{0} & \Delta_{f_n, f_n} & \mathbf{0} \\ \Delta_{\delta, \theta_n} & \Delta_{\delta, \tilde{\theta}_m} & \mathbf{0} & \Delta_{\delta, \delta} \end{bmatrix}$$

To compute the inverse matrix of M , we use (S1) again. By partitioning M and defining A' , B' , C' and D' similarly, we can compute M' as follows.

$$M' = A' - B'D'^{-1}C'$$

$$= \begin{bmatrix} \Delta_{\theta_n, \theta_n} - \Delta_{\theta_n, \delta} \Delta_{\delta, \delta}^{-1} \Delta_{\delta, \theta_n} & \Delta_{\theta_n, \tilde{\theta}_m} - \Delta_{\theta_n, \delta} \Delta_{\delta, \delta}^{-1} \Delta_{\delta, \tilde{\theta}_m} & \mathbf{0} \\ \Delta_{\tilde{\theta}_m, \theta_n} - \Delta_{\tilde{\theta}_m, \delta} \Delta_{\delta, \delta}^{-1} \Delta_{\delta, \theta_n} & \Delta_{\tilde{\theta}_m, \tilde{\theta}_m} - \Delta_{\tilde{\theta}_m, \delta} \Delta_{\delta, \delta}^{-1} \Delta_{\delta, \tilde{\theta}_m} & \mathbf{0} \\ \mathbf{0} & \mathbf{0} & \Delta_{f_n, f_n} \end{bmatrix}$$

We partition M' and define A'' , B'' , C'' and D'' using the same procedure. We find that the off-diagonal blocks B'' and C'' are zero-matrices. This simplifies the calculation, as $M'' = A''$ and thus $M''^{-1} = A''^{-1}$.

Next, we partition A'' (the upper-left block of 2×2 of M') into its components:

$$A''' = \Delta_{\theta_n, \theta_n} - \Delta_{\theta_n, \delta} \Delta_{\delta, \delta}^{-1} \Delta_{\delta, \theta_n}$$

$$B''' = \Delta_{\theta_n, \tilde{\theta}_m} - \Delta_{\theta_n, \delta} \Delta_{\delta, \delta}^{-1} \Delta_{\delta, \tilde{\theta}_m}$$

$$C''' = \Delta_{\tilde{\theta}_m, \theta_n} - \Delta_{\tilde{\theta}_m, \delta} \Delta_{\delta, \delta}^{-1} \Delta_{\delta, \theta_n}$$

$$D''' = \Delta_{\tilde{\theta}_m, \tilde{\theta}_m} - \Delta_{\tilde{\theta}_m, \delta} \Delta_{\delta, \delta}^{-1} \Delta_{\delta, \tilde{\theta}_m}$$

Applying (S1), we can compute M''^{-1} . In addition, adopting the notation for our target

matrix $\hat{\Sigma}$, we define the resulting components as follows:

$$M''^{-1} = \begin{bmatrix} M'''^{-1} & -M'''^{-1}B'''D'''^{-1} \\ -D'''^{-1}C'''M'''^{-1} & D'''^{-1} + D'''^{-1}C'''M'''^{-1}B'''D'''^{-1} \end{bmatrix} \quad (S3)$$

$$\equiv \begin{bmatrix} \hat{\Sigma}_{\theta_n, \theta_n} & \hat{\Sigma}_{\theta_n, \tilde{\theta}_m} \\ \hat{\Sigma}_{\tilde{\theta}_m, \theta_n} & \hat{\Sigma}_{\tilde{\theta}_m, \tilde{\theta}_m} \end{bmatrix}$$

where $M''' = A''' - B'''D'''^{-1}C'''$. Similarly, we can compute M'^{-1} and M^{-1}

$$M'^{-1} = \begin{bmatrix} M''^{-1} & \mathbf{0} \\ \mathbf{0} & D''^{-1} \end{bmatrix} = \begin{bmatrix} M''^{-1} & \mathbf{0} \\ \mathbf{0} & \hat{\Sigma}_{f_n, f_n} \end{bmatrix}$$

where $D'' = \Delta_{f_n, f_n}$ and we define $\hat{\Sigma}_{f_n, f_n} \equiv D''^{-1}$.

$$-M'^{-1}B'D'^{-1} = - \begin{bmatrix} \hat{\Sigma}_{\theta_n, \theta_n} & \hat{\Sigma}_{\theta_n, \tilde{\theta}_m} & \mathbf{0} \\ \hat{\Sigma}_{\tilde{\theta}_m, \theta_n} & \hat{\Sigma}_{\tilde{\theta}_m, \tilde{\theta}_m} & \mathbf{0} \\ \mathbf{0} & \mathbf{0} & \hat{\Sigma}_{f_n, f_n} \end{bmatrix} \begin{bmatrix} \Delta_{\theta_n, \delta} \\ \Delta_{\tilde{\theta}_m, \delta} \\ \mathbf{0} \end{bmatrix} \Delta_{\delta, \delta}^{-1} \quad (S4)$$

$$= \begin{bmatrix} -(\hat{\Sigma}_{\theta_n, \theta_n} \Delta_{\theta_n, \delta} + \hat{\Sigma}_{\theta_n, \tilde{\theta}_m} \Delta_{\tilde{\theta}_m, \delta}) \Delta_{\delta, \delta}^{-1} \\ -(\hat{\Sigma}_{\tilde{\theta}_m, \theta_n} \Delta_{\theta_n, \delta} + \hat{\Sigma}_{\tilde{\theta}_m, \tilde{\theta}_m} \Delta_{\tilde{\theta}_m, \delta}) \Delta_{\delta, \delta}^{-1} \\ \mathbf{0} \end{bmatrix}$$

As before, we define the upper block of (S4) $\hat{\Sigma}_{\theta_n, \delta}$ and the middle block as $\hat{\Sigma}_{\tilde{\theta}_m, \delta}$. Note that $-D'^{-1}C'M'^{-1}$ is the transpose of (S4).

By using result of (S3),

$$D'^{-1} + D'^{-1}C'M'^{-1}B'D'^{-1} = \Delta_{\delta, \delta}^{-1} - \Delta_{\delta, \delta}^{-1}(\Delta_{\delta, \theta_n} \hat{\Sigma}_{\theta_n, \delta} + \Delta_{\delta, \tilde{\theta}_m} \hat{\Sigma}_{\tilde{\theta}_m, \delta}) \Delta_{\delta, \delta}^{-1}$$

$$\equiv \hat{\Sigma}_{\delta, \delta}$$

Summarizing these results, we have

$$M^{-1} = \begin{bmatrix} \hat{\Sigma}_{\theta_n, \theta_n} & \hat{\Sigma}_{\theta_n, \tilde{\theta}_m} & \mathbf{0} & \hat{\Sigma}_{\theta_n, \delta} \\ \hat{\Sigma}_{\tilde{\theta}_m, \theta_n} & \hat{\Sigma}_{\tilde{\theta}_m, \tilde{\theta}_m} & \mathbf{0} & \hat{\Sigma}_{\tilde{\theta}_m, \delta} \\ \mathbf{0} & \mathbf{0} & \hat{\Sigma}_{f_n, f_n} & \mathbf{0} \\ \hat{\Sigma}_{\delta, \theta_n} & \hat{\Sigma}_{\delta, \tilde{\theta}_m} & \mathbf{0} & \hat{\Sigma}_{\delta, \delta} \end{bmatrix}$$

This matrix corresponds to the upper-left 4×4 block of $\hat{\Sigma}$. Finally, we compute the remaining blocks of $\hat{\Sigma}$.

$$-M^{-1}BD^{-1} = \begin{bmatrix} \hat{\Sigma}_{\theta_n, \theta_n} T_n \\ \hat{\Sigma}_{\tilde{\theta}_m, \theta_n} T_n \\ \hat{\Sigma}_{f_n, f_n} \\ \hat{\Sigma}_{\delta, \theta_n} T_n \end{bmatrix} \equiv \begin{bmatrix} \hat{\Sigma}_{\theta_n, y_n} \\ \hat{\Sigma}_{\tilde{\theta}_m, y_n} \\ \hat{\Sigma}_{f_n, y_n} \\ \hat{\Sigma}_{\delta, y_n} \end{bmatrix}. \quad (\text{S5})$$

This matrix corresponds to the upper-right 4×1 block of $\hat{\Sigma}$. The lower-left block of $\hat{\Sigma}$ is equivalent to the transpose of (S5).

$$D^{-1} + D^{-1}CM^{-1}BD^{-1} = s_\epsilon^{-1}I_n + T_n \hat{\Sigma}_{\theta_n, y_n} + \hat{\Sigma}_{f_n, y_n}$$

This matrix corresponds to the lower-right scalar block of $\hat{\Sigma}$.

S2 Data Generation Process for Experiment

In this section, we detail data generation process used in the Experiments section. These settings are from Nie and Wager (2020). In our simulation study, we set sample size of training data at $N = \{200, 500, 1000\}$ and test data at $M = 500$. In all scenarios (Setup A to D), \mathbf{X}_i, T_i and Y_i are sampled as follows:

$$Y_i = \theta(\mathbf{X}_i)T_i + f(\mathbf{X}_i) + \epsilon_i, \quad T_i | \mathbf{X}_i \sim \text{Ber}(e(\mathbf{X}_i)),$$

where $\mathbf{X}_i \sim p(\mathbf{x})$ and $\mathbf{X}_i \in \mathcal{R}^6$. In Nie and Wager (2020), the baseline function $f(\mathbf{X})$ is formulated as $f(\mathbf{X}_i) = b(\mathbf{X}) - 0.5 \theta(\mathbf{X})$. In each scenario, the formulation of $p(\mathbf{x})$, $e(\mathbf{X})$, $\theta(\mathbf{X})$ and $b(\mathbf{X})$ are set differently.

- **(Setup A)** This setting uses smooth θ and f , where both specifications use common variables (X_1 and X_2), described as

$$e(\mathbf{X}) = \text{trim}_{0.1}\{\sin(\pi X_1 X_2)\}, \quad \theta(\mathbf{X}) = \frac{1}{2}(X_1 + X_2),$$

$$b(\mathbf{X}) = \sin(\pi X_1 X_2) + 2(X_3 - 0.5)^2 + X_4 + 0.5X_5,$$

where $\text{trim}_\eta(x) = \max\{\eta, \min(x, 1 - \eta)\}$. Here $X_{ik} \sim U(0, 1)$, independently for $k = 1, \dots, 6$.

- **(Setup B)** This setting uses constant $e(\mathbf{X})$, so all units have equivalent probability for assignment.

$$e(\mathbf{X}) = 0.5, \quad \theta(\mathbf{X}) = X_1 + \log(1 + e^{X_2}),$$

$$b(\mathbf{X}) = \max\{X_1 + X_2, X_3, 0\} + \max\{X_4, X_5\},$$

where $\mathbf{X} \sim \mathcal{N}(\mathbf{0}, \mathbf{I})$.

- **(Setup C)** This setting uses constant function for $\theta(\mathbf{X})$. In this setting, there is no heterogeneity for treatment effects.

$$e(\mathbf{X}) = \frac{1}{1 + e^{X_2 + X_3}}, \quad \theta(\mathbf{X}) = 1, \quad b(\mathbf{X}) = 2 \log(1 + e^{X_1 + X_2 + X_3}),$$

where $\mathbf{X} \sim \mathcal{N}(\mathbf{0}, \mathbf{I})$.

- **(Setup D)** This setting uses non-differentiable and structurally similar functions for $\theta(\mathbf{X})$ and $f(\mathbf{X})$.

$$e(\mathbf{X}) = \frac{1}{1 + e^{-X_1 - X_2}}, \quad \theta(\mathbf{X}) = \max\{X_1 + X_2 + X_3, 0\} - \max\{X_4 + X_5, 0\},$$

$$b(\mathbf{X}) = \frac{1}{2}(\max\{X_1 + X_2 + X_3, 0\} - \max\{X_4 + X_5, 0\}),$$

where $\mathbf{X} \sim \mathcal{N}(\mathbf{0}, \mathbf{I})$.

S3 Additional Experimental Results

Here we show additional results of the simulation study. In Section 3, we investigate Setup A and C. In Setup B and D, approximate trends of results are consistent.

The Tables S1, S2, S3 and S4 show the detailed results of the simulation study. PPK produces shorter credible interval length (CI length) and smaller empirical coverage rate (Coverage) than the simple local approximation methods. This is likely because the added pseudo-data as additional samples in each local model, leading to tighter confidence intervals and, as a result, lower coverage.

	$N = 200$			$N = 500$			$N = 1000$		
	MSE	CI length	Coverage	MSE	CI length	Coverage	MSE	CI length	Coverage
PPK (K2)	0.1	1.26	0.86	0.06	0.88	0.84	0.05	0.66	0.79
PPK (K5)	0.08	1.47	0.9	0.05	1.03	0.88	0.04	0.87	0.83
PPK (K10)	0.08	1.81	0.95	0.05	1.33	0.94	0.04	1.06	0.88
GP (K2)	0.15	1.52	0.91	0.08	1.06	0.91	0.06	0.8	0.86
GP (K5)	0.21	2.13	0.94	0.12	1.55	0.94	0.09	1.25	0.92
GP (K10)	0.24	2.65	0.95	0.17	2.08	0.97	0.12	1.71	0.96
GP	0.13	1.06	0.8	0.07	0.78	0.83	0.05	0.62	0.78
BCF	0.09	0.78	0.79	0.07	0.61	0.75	0.05	0.57	0.76

Table S1: Performance metrics for Setting A

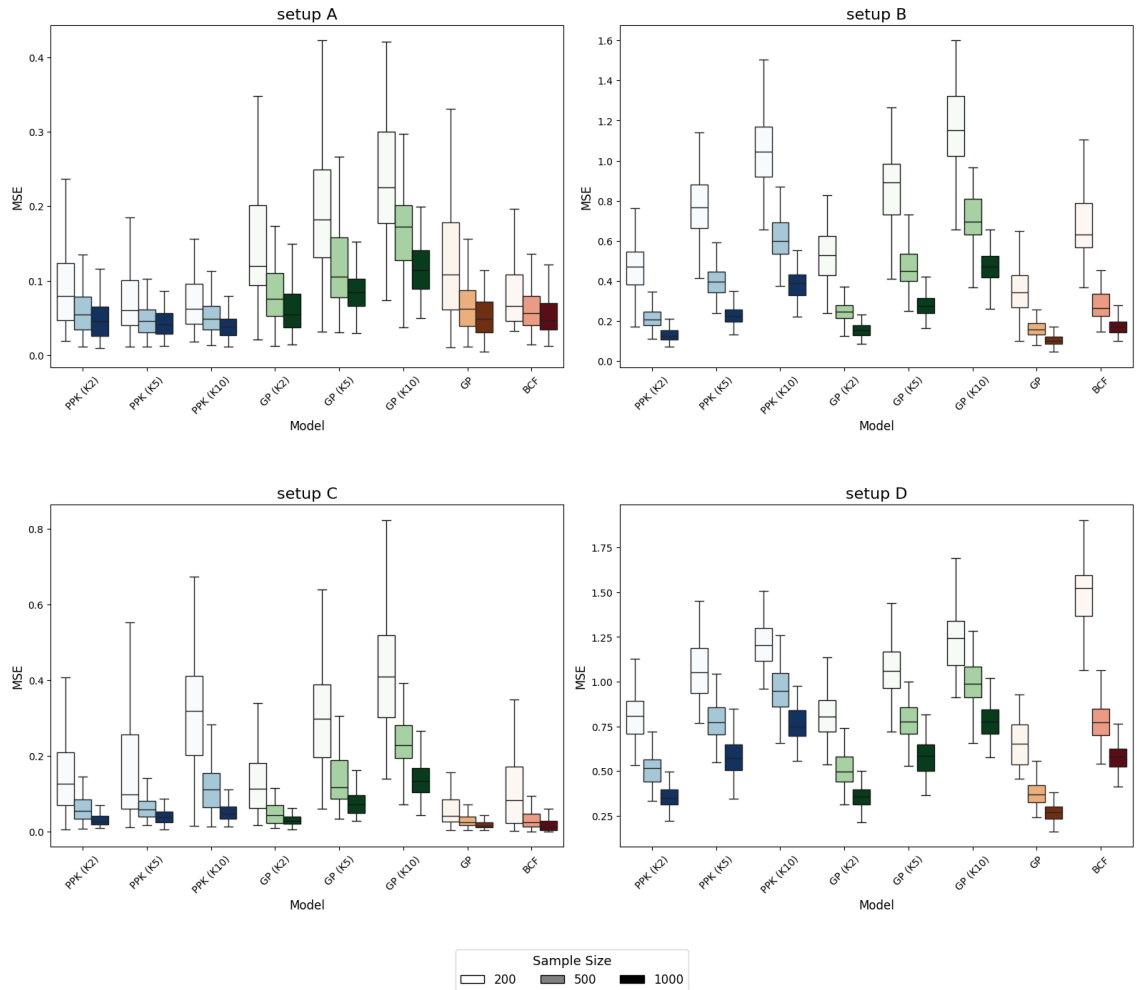


Figure S1: MSEs on all DGP settings

	N = 200			N = 500			N = 1000		
	MSE	CI length	Coverage	MSE	CI length	Coverage	MSE	CI length	Coverage
PPK (K2)	0.48	1.76	0.81	0.22	1.46	0.91	0.13	1.23	0.95
PPK (K5)	0.78	1.76	0.67	0.4	1.46	0.76	0.23	1.27	0.85
PPK (K10)	1.05	1.93	0.62	0.61	1.57	0.68	0.39	1.36	0.74
GP (K2)	0.54	2.01	0.84	0.25	1.61	0.91	0.15	1.33	0.94
GP (K5)	0.86	2.42	0.82	0.47	1.93	0.86	0.28	1.61	0.9
GP (K10)	1.15	2.83	0.81	0.71	2.3	0.84	0.47	1.92	0.86
GP	0.37	1.77	0.88	0.16	1.4	0.95	0.11	1.14	0.96
BCF	0.7	1.55	0.68	0.28	1.39	0.83	0.18	1.14	0.85

Table S2: Performance metrics for Setting B

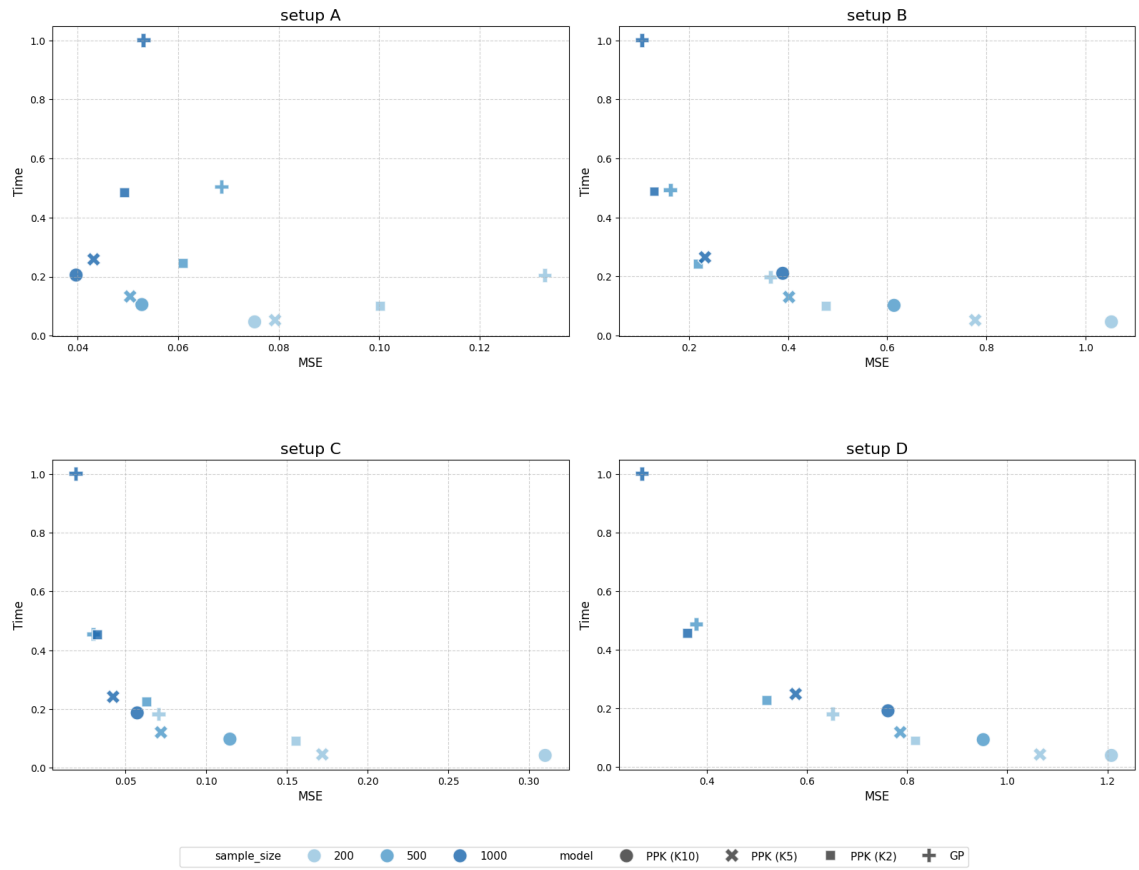


Figure S2: Computation time and MSEs on all DGP settings

	$N = 200$			$N = 500$			$N = 1000$		
	MSE	CI length	Coverage	MSE	CI length	Coverage	MSE	CI length	Coverage
PPK (K2)	0.16	1.19	0.85	0.06	0.85	0.9	0.03	0.69	0.95
PPK (K5)	0.17	1.23	0.87	0.07	0.8	0.87	0.04	0.62	0.86
PPK (K10)	0.31	1.49	0.77	0.11	0.92	0.84	0.06	0.63	0.82
GP (K2)	0.15	1.54	0.96	0.05	1.09	0.99	0.03	0.87	0.98
GP (K5)	0.32	2.07	0.96	0.14	1.44	0.96	0.08	1.11	0.94
GP (K10)	0.42	2.55	0.96	0.24	1.85	0.95	0.14	1.4	0.94
GP	0.07	1.29	0.98	0.03	0.94	1.0	0.02	0.75	0.99
BCF	0.13	1.06	0.84	0.04	0.77	0.95	0.02	0.54	0.95

Table S3: Performance metrics for Setting C

	$N = 200$			$N = 500$			$N = 1000$		
	MSE	CI length	Coverage	MSE	CI length	Coverage	MSE	CI length	Coverage
PPK (K2)	0.82	1.99	0.75	0.52	1.64	0.77	0.36	1.36	0.76
PPK (K5)	1.07	2.0	0.67	0.79	1.73	0.69	0.58	1.48	0.69
PPK (K10)	1.21	2.17	0.66	0.95	1.89	0.67	0.76	1.61	0.66
GP (K2)	0.81	2.16	0.78	0.52	1.74	0.8	0.37	1.42	0.78
GP (K5)	1.08	2.55	0.78	0.78	2.11	0.78	0.58	1.74	0.77
GP (K10)	1.22	2.88	0.8	1.0	2.47	0.78	0.78	2.04	0.77
GP	0.65	2.08	0.83	0.38	1.64	0.84	0.27	1.38	0.84
BCF	1.49	1.49	0.58	0.78	1.87	0.74	0.59	1.71	0.77

Table S4: Performance metrics for Setting D

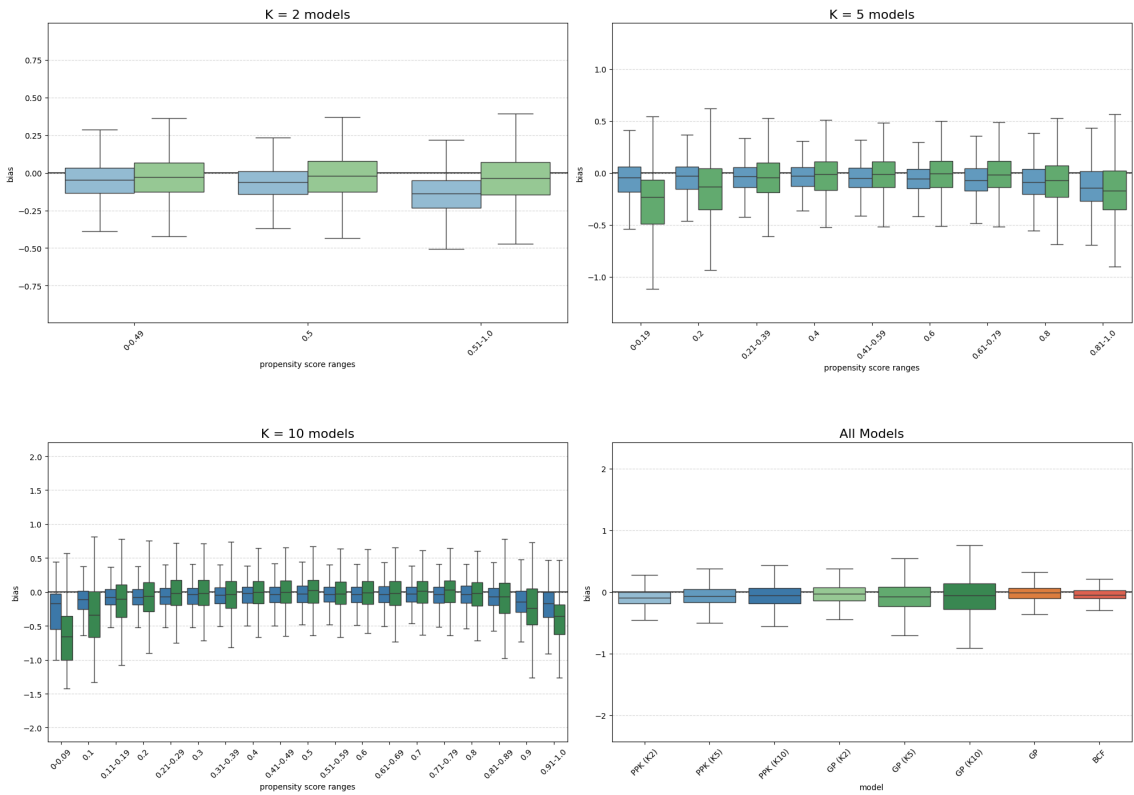


Figure S3: Comparison of HTE estimation bias near partition boundaries on Setup C. The plots show the average bias for data points within a ± 0.01 margin of the specified split points. The panels represent $K = 2$ (top-left), $K = 5$ (top-right), and $K = 10$ (bottom-left), with the bottom-right panel summarizing the bias across all K settings and other methods.